Int. J. Electrochem. Sci., 12 **(2017)** 8695 – 8707, doi: 10.20964/2017.09.59

International Journal of
ELECTROCHEMICAL
SCIENCE
www.electrochemsci.org

Surface Modification through Biocompatible Coatings of Tricalcium Phosphate on Magnesium to Obtain Uniform Degradation Behaviour

W. Aperador[1,*], *A. Delgado*[1], *J. C. Caicedo*[2]

[1] School of Engineering, Universidad Militar Nueva Granada, Bogotá-Colombia
[2] Tribology Polymers, Powder Metallurgy and Processing of Solid Recycled Research Group
Universidad del Valle, Cali – Colombia
[*]E-mail: g.ing.materiales@gmail.com

Received: 19 April 2017 / *Accepted:* 19 July 2017 / *Published:* 13 August 2017

In this work, the surface of a Mg-8Er alloy was modified by coating with tricalcium phosphate via electrochemical deposition to make the alloy more resistant to corrosion by body fluids. The goal is to improve the integration of implants, avoid the rejection of cytotoxic products, and optimize bone regeneration. The morphologies of the substrate and the coating were examined using X-ray diffraction (XRD). Corrosion tests were performed using potentiodynamic polarization techniques and electrochemical impedance spectroscopy (EIS) under conditions similar to those of the human body, which in this case is an aqueous solution of oxygen and various salts, such as sodium chloride (NaCl), magnesium chloride (MgCl), potassium chloride (KCl) and glucose. The solution had an overall pH of approximately 7.4. The immersion test results show that the calcium phosphate coating can mitigate the corrosion of the Mg alloy (substrate). Scanning electron microscopy (SEM) revealed that the tricalcium phosphate coating can mitigate the general corrosion of the Mg-8Er alloy.

Keywords: Magnesium, biocompatibility, corrosion, tricalcium phosphate, coating.

1. INTRODUCTION

At present, it is necessary to obtain new biocompatible and biodegradable materials as substitutes for titanium and stainless steel to assist in healing bone fractures because these materials release metallic ions that are harmful to the body. Additionally, when using these materials, two surgeries are required: one to place the material and another to remove it [1]. Magnesium (Mg) and its alloys have been studied for use as biodegradable/biocompatible materials because they play a fundamental role in osteosynthesis. Additionally, because of the biodegradation properties of Mg, surgery is no longer required to remove the implant, only to place it, thereby reducing the recovery time and avoiding complications such as infections and rehealing. In addition, the properties of Mg are similar to those of bone [2]. The material used in this work is the Mg alloy Mg-8Er. Mg is a light metal that degrades very quickly via electrochemical corrosion, which means that without surface modifications, this material is not suitable for assisting in orthopaedic recovery. Erbium (Er) is a metal that has few uses [3]. In this case, blending Er with pure Mg results in a Mg-Er alloy that has superior material properties and that is easier to machine than pure Mg [4]. A tricalcium phosphate coating is used to impart the material with greater compatibility, improve its mechanical integrity, and stimulate a better bone matrix, as calcium phosphate is the major component of bone tissue [5].

Bone fractures require special care to heal properly; in some cases, a plaster cast and certain precautions are sufficient, but for severe injuries, the treatment becomes more delicate. Many fractures require the placement of implants, such as screws, nails or plates, to keep the bone fixed during healing [6].

These implants are fabricated from stainless steel or titanium because these materials possess extraordinary mechanical properties. However, these materials also decrease biocompatibility and cause inflammation and infections; moreover, these metals and alloys experience corrosion in the human body due to their microstructural properties, surface state and carbon and hydrogen contents [7].

Conceptually, a biomaterial is a substance (different from a drug or medicine) or a combination of substances that can be used for a period of time as an entire system or as part of a system to treat or replace an organ, tissue, or body function [8]. In other words, a non-living material is used as a medical device with the goal of interacting with a biological system. Magnesium is considered to be biodegradable because its properties are very similar to those of bone; calcium is one of the major components in the human body and degrades under physiological conditions via electrochemical corrosion [9]. Although these new materials are compatible with the human body, Mg is very susceptible to corrosion and can degrade prior to full tissue recovery. Therefore, it is necessary to perform superficial modifications to maintain mechanical integrity and to ensure that there are no limits on the orthopaedic applications [10].

The purpose of this work is to perform superficial modifications to the Mg-8Er alloy using a coating of tricalcium phosphate, evaluate its degradation behaviour in simulated electrolytes and determine the degradation delay of the material.

2. EXPERIMENTAL DETAILS

2.1 Alloy

The alloy used in this work is Mg-8Er. The composition of this alloy was determined by X-ray fluorescence and is shown in Table 1. Such alloys have become important in the biomedical industry for manufacturing surgical instruments, with the vision of creating implants that have greater compatibility with the human body and a friendlier interaction with bone tissue because the superior mechanical properties of conventional implants induce significant wear during their residence time. According to the above, alternatives are being studied to improve corrosion resistance through depositing a coating on the metal surface of magnesium alloys and through surface treatments.

Table 1. Composition of the alloy used as the substrate.

Alloy (wt. %)	Mg	Er	Cu	Fe	Ni
Mg–8Er	91.6608	8.3263	0.0051	0.0040	0.0038

2.2 Tricalcium phosphate coating

The technique used was the electrodeposition of β-tricalcium phosphate coatings via an anodic oxidation process in an equivalent solution of hydrochloric acid, sulfuric acid and distilled water. This process was performed to adhere the coating to the substrate. Subsequently, cathodic electrodeposition was performed to obtain a β-tricalcium phosphate coating film. Conventional electrolysis was used to deposit layers of calcium phosphate on the metallic substrate based on the cathodic reduction of water, thus leading to a local pH increase that can be leveraged to precipitate the calcium and phosphate ions present in the solution and obtain an insoluble adherent layer of calcium phosphate on the metal. The morphology, composition, thickness and structural characteristics of the coating depend on the temperature of the electrolyte, the applied current of 310 mA/s, the deposition time of 2 hours and the agitation speed of 220 RPM.

2.3 Characterization via XRD and SEM

The structures of the films were investigated using X-ray diffraction (XRD) analysis, which was conducted using a PANalytical Empyrean X-ray diffractometer with Cu Kα radiation ($\lambda = 1.54060$ Å) in the Bragg-Brentano configuration with a counting time of 1 second per step and a step size of 0.03°. The phases were identified using the ICCD database accessed with the X’Pert High Score software. The surface was observed under high vacuum using a JEOL NeoScope JCM-5000 scanning electron microscope operating at 10 kV.

2.4 EIS

Electrochemical impedance spectroscopy (EIS) measurements were performed because this technique allows the study of the mechanisms and kinetics of the corrosion of metal/electrolyte and metal/coating/electrolyte systems. This is a particularly useful technique: it hardly disturbs the system being studied and does not interfere with transport phenomena because the electrochemical process occurs through the system response when disturbed with a sinusoidal potential of 10 mV and a frequency range of 100 kHz to 0.1 Hz. For the EIS study, the samples were prepared by deburring one side of the Mg-8Er alloy to grade P1000. The area exposed to the aggressive medium was approximately 2 cm^2. Upon coating, no surface preparation was applied after the deposition.

The first EIS measurement, called 14 days, was evaluated after 24 hours, allowing the stabilization of open circuit potential. The electrolyte used to simulate conditions of human body fluid was the solution of ringer's during the 90 days evaluated, the chemical composition of the solution in (g / l) 9 of NacL, 0.24 $CaCl_2$, 0.43 KCl and 0.2 $NaHCO_3$ with a pH Of 7.2.

3. RESULTS

3.1 X-ray diffraction (XRD)

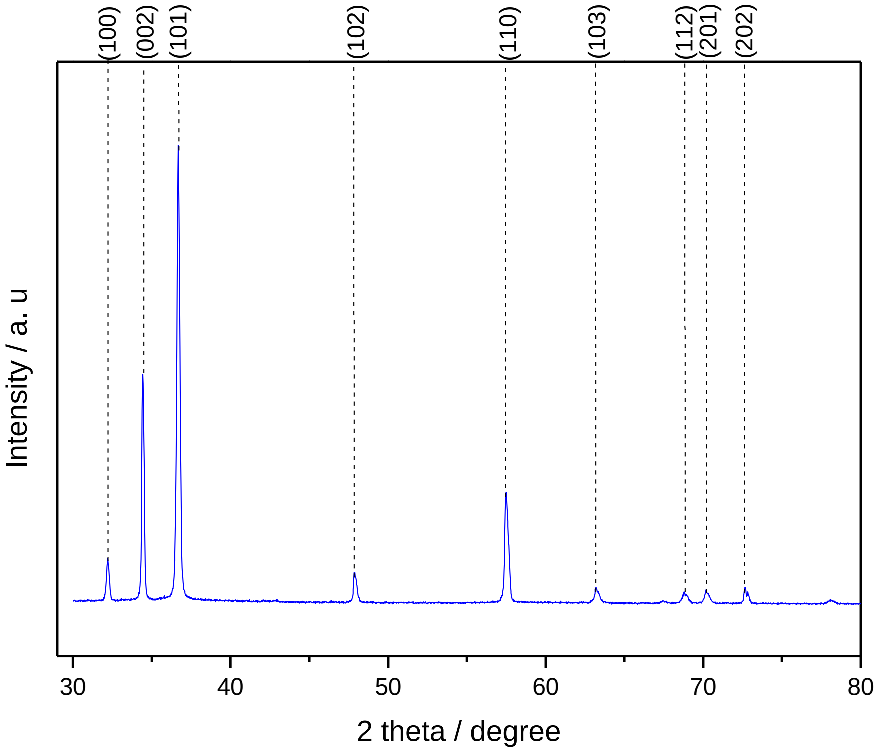

Figure 1. X-ray diffraction pattern of the Mg-8Er alloy

Figure 1 presents a crystallographic study of the magnesium samples at 14, 28 and 90 days, which was conducted following the simulated corrosion tests. However, no significant changes in the results were obtained as a function of time; thus, the test was stopped at 90 days. From the diffraction peaks, we observed a significant amount of magnesium, the greatest intensity of which corresponds to the Mg (101) plane of metallic magnesium, accompanied by families of characteristic planes such as Mg (002), Mg (102), Mg (201) and Mg (103), which describe a compact hexagonal structure (HCP) [11]. Nevertheless, for the coating of magnesium oxide, a greater intensity is evident in the peak corresponding to the MgO (100) plane, accompanied by the family of MgO (110) and MgO (202) planes with a face-centred cubic structure (FCC). In addition, the XRD pattern presents a characteristic peak of magnesium fluoride corresponding to the Mg_2F_2 (112) plane, indicating a body-centred tetragonal lattice (tetragonal-I). The presence of this peak is attributed to the interactions of the material with the electrolyte, which in turn is attributed to atomic diffusion from the substrate-electrolyte interface [12].

For the crystallographic simulations of the structure of the magnesium oxide (MgO) coating, it was necessary to use the experimental results as a basis for the characterization techniques performed in this study. The morphology determined using SEM enables the determination of magnesium oxides on the surface that correspond to the types of crystal structures and the values of the lattice parameters experimentally obtained using XRD. The atomic radii of the elements presented here depend on the type of link between them and on the occupation of the atoms, which is determined by performing a structure analysis corresponding to the coordination number of the FCC structure and the Miller indices [13]. The lattice parameter used is 4.206 Å, and the sites occupied by the magnesium atoms correspond to the octahedral positions of the cell and the ratio of magnesium to oxygen atoms.

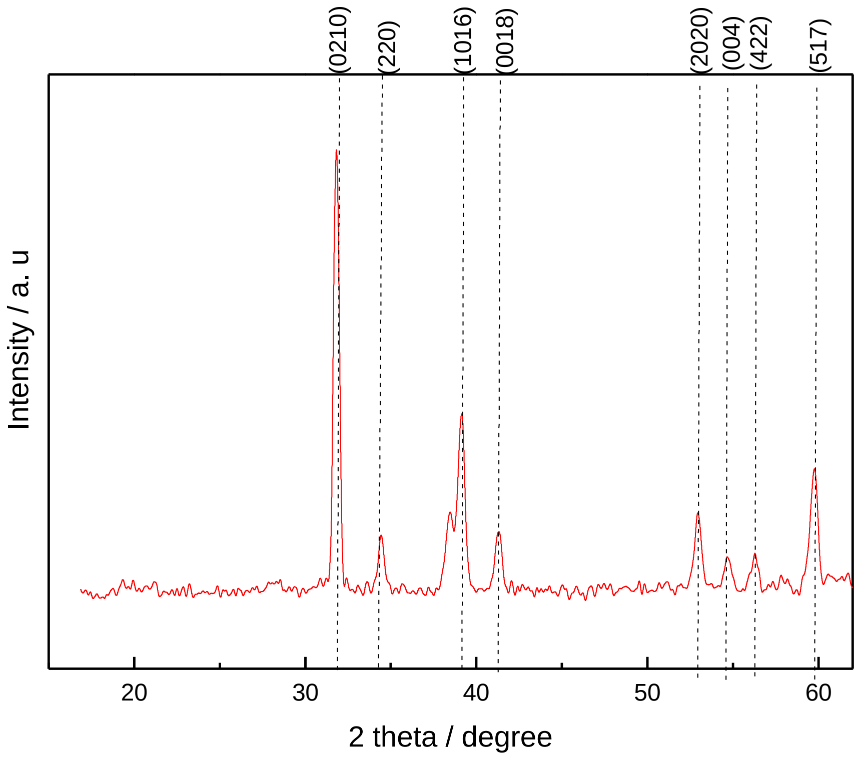

Figure 2. X-ray diffraction (XRD) patterns of tricalcium phosphate.

Figure 2 presents the diffractograms that correspond to the characteristic patterns of the tricalcium phosphate phase from the different coatings synthesized after 14, 28 and 90 days. These diffractograms were obtained at low angles of incidence, where there is a response from the interaction between the incident ray and the coatings examined for all the compositions. In addition, a significant change in the intensity of some peaks implies that some crystallographic orientations grow at the expense of others due to the inclusion of the polysaccharide bond in the crystalline structure of the tricalcium phosphate [14]. According to the XRD patterns, the present phases are identified as β-tricalcium phosphate. The corresponding diffraction peaks are very sharp, indicating high crystallinity of the two phases and that the obtained crystal size is relatively large. It is well known that this two-phase calcium phosphate is required for use as a biomaterial due to the greater biodegradability of the β-TCP phase [15].

3.2 Electrochemical impedance spectroscopy (EIS)

Figure 3 presents the impedance spectrum of the organic coating applied on the metal Mg-8Er substrate in contact with a simulated physiological solution. The film was evaluated until 90 days of immersion passed, during which time the protective film was periodically evaluated [16]. The impedance diagram shows the interactions between the coating and the substrate as a function of time. The behaviour of the coating materials is obtained as a function of the impedance, and the obtained performance is classified as being adequate because it possesses a resistance of greater than 10^5 Ω.cm^2 [17].

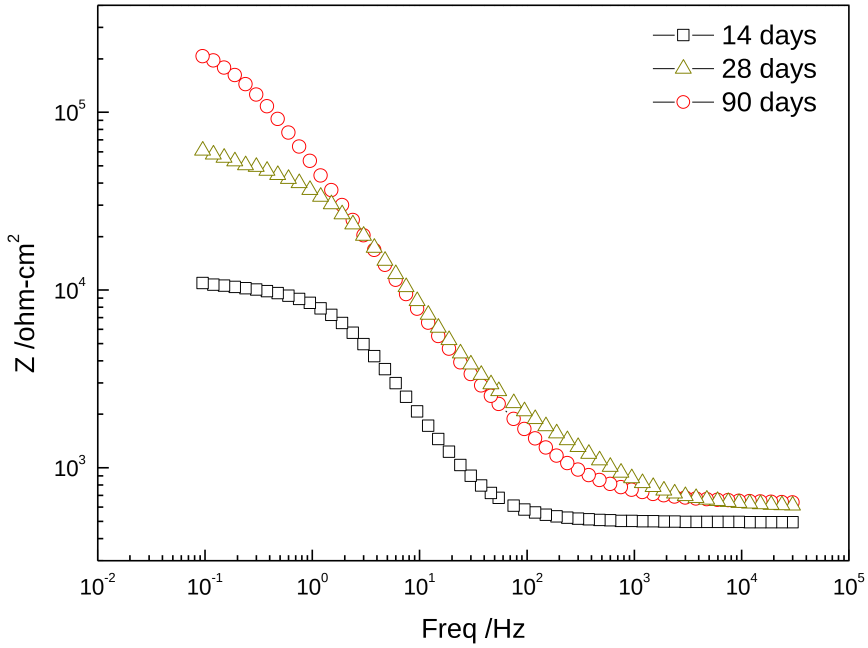

Figure 3. Bode diagram appropriate for the coatings, where an increase in the impedance as a function of time is observed.

Figure 4 shows the Bode diagram corresponding to the phase angle versus the logarithm of the frequency. As time increases, there is an expansion of the frequency range, where the contribution of the imaginary part to the impedance is significant. As shown, the phase angle is not zero.

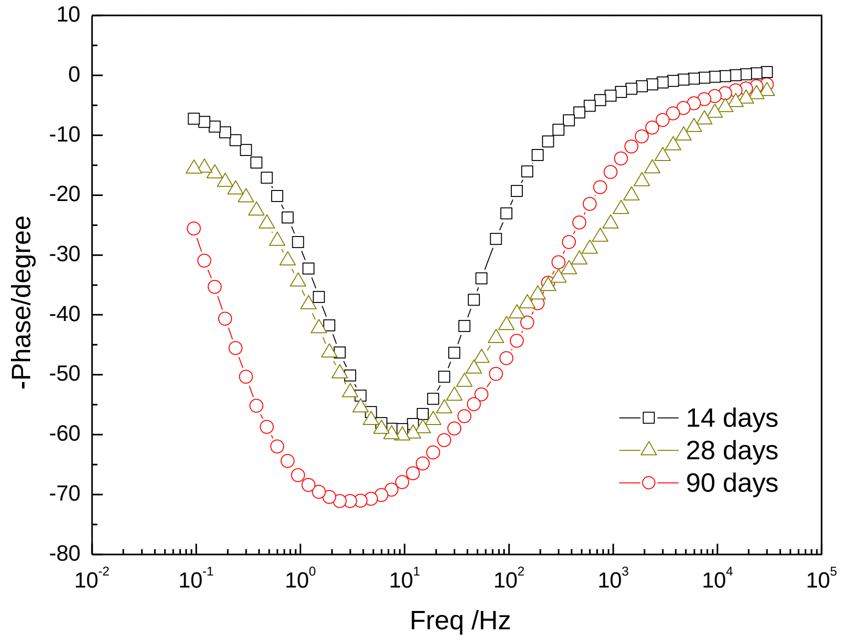

Figure 4. Bode diagram for the phase angle versus the logarithm of the frequency for the tricalcium phosphate coating; a change in capacitance is observed as time increases.

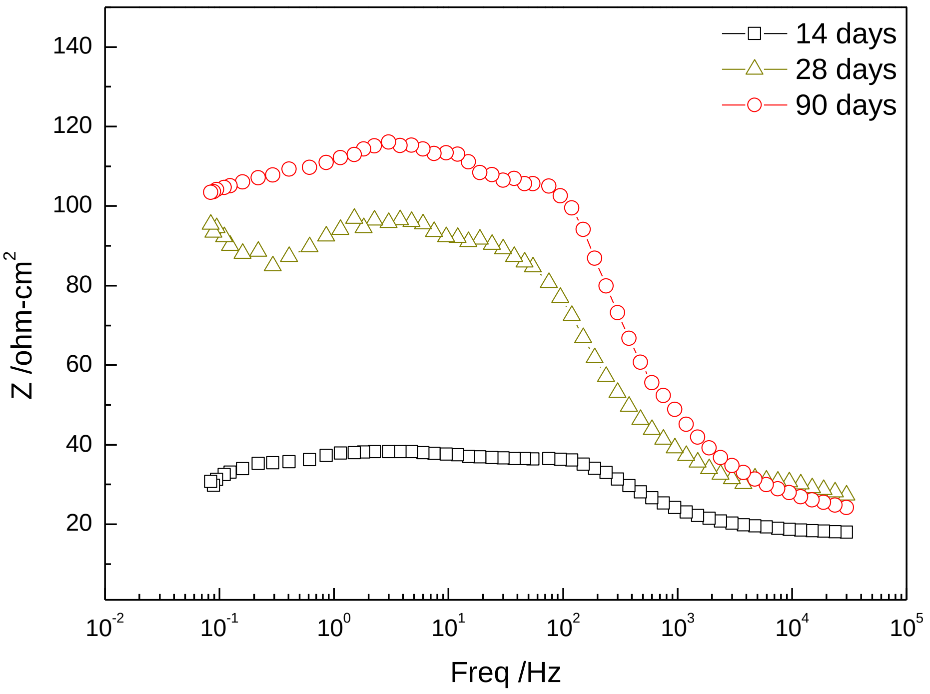

Figure 5. Impedance diagram corresponding to the substrate and evaluated at 14, 28 and 90 days of immersion in a simulated physiological solution.

Figure 5 shows the substrate and its response as a function of time by comparing the impedance diagram against the logarithm of the frequency. A low total impedance response is obtained compared to the tricalcium phosphate coating. The electrolyte permeates areas where the molecular bonds are weak and creates an ion-conducting pathway [18]. Consequently, a thin layer of NaCl forms at the metal/magnesium oxide interface, in which parts of the metal serve as anodes and cathodes. The substrate oxidizes at the anodic sites, and the oxygen uptake accelerates the reactions at the cathodic sites, increasing the pH and decreasing the oxide adhesion [19].

Figure 6 shows the recorded capacitance data, which show that there is absorption at high frequencies, that transfer processes occur at intermediate frequencies between 10^2 Hz and 10^3 Hz, and that diffusion processes are observed at a low frequency of 0.1 Hz.

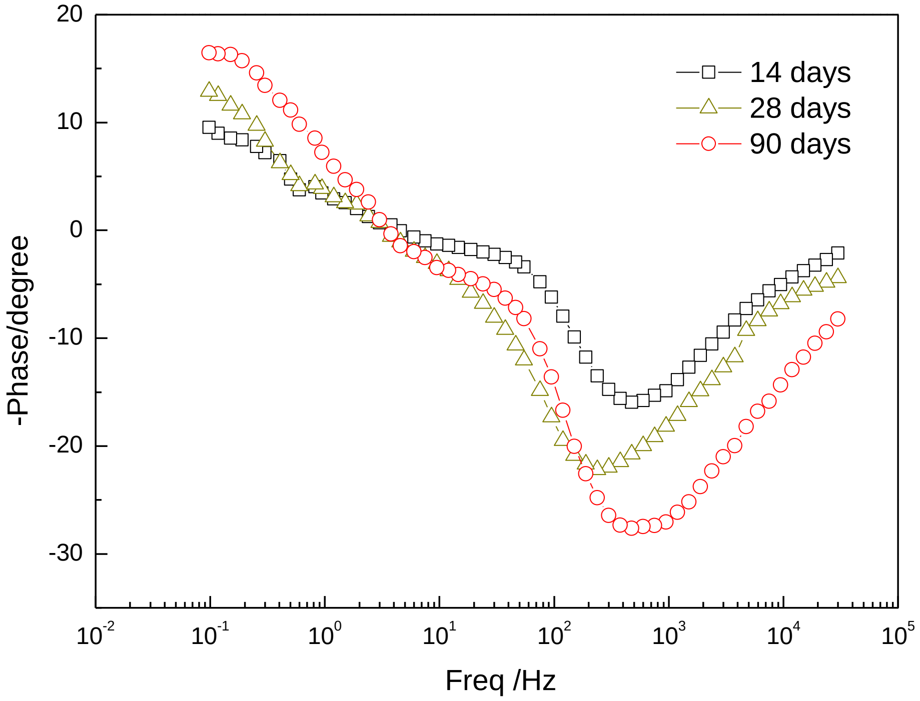

Figure 6. Phase angle diagram corresponding to the substrate and evaluated at 14, 28 and 90 days of immersion in a simulated physiological solution; an increase in capacitance is observed as a function of time.

Figure 7 shows the equivalent circuit corresponding to the impedance data for the coating-substrate system. This is a simple circuit consisting of a double layer resistance and a double layer capacitance of the coating. From this circuit, we infer that the coating functions as a perfect barrier [20]. The capacitance within the equivalent circuit is replaced by a constant phase element.

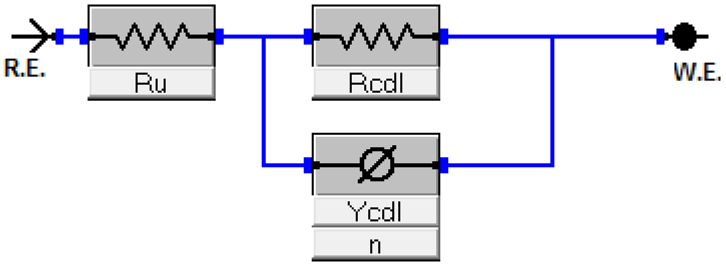

Figure 7. Equivalent circuit corresponding to the modelling used to adjust the coating data.

Figure 8 shows the equivalent circuit used to simulate the behaviour of the substrate after exposure to the simulated biological fluid. The ions and oxygen reach the substrate and form electrochemical corrosion sites at the interface, which is represented in the equivalent circuit by the double layer capacitance, Ccorr, and transfer resistance, Rcorr [21]. After an intensive attack, the corrosion products are represented in the equivalent circuit as Rdiff. To better understand the elements that compose the equivalent circuit, we can associate each element with a physical phenomenon within the substrate system/magnesium oxides in contact with the working solution. Rpo is referred to as the pore resistance and is related to how ionic conduction pathways form within the metal. Cpo is the capacitance associated with the structure of the magnesium oxide. Rcorr is the polarization resistance of the metal surface in contact with the ion conduction pathways, and Ccorr is the respective capacitance of this contact [21].

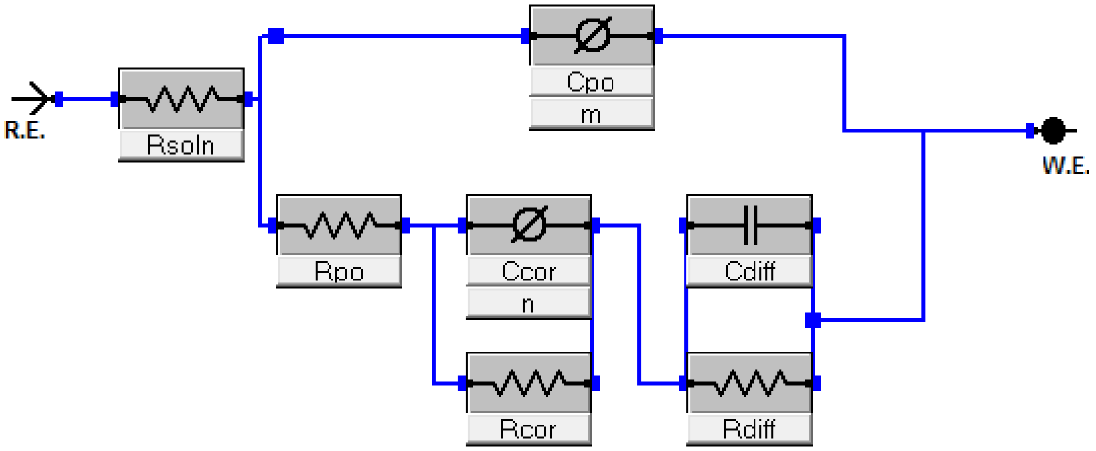

Figure 8. Equivalent circuit corresponding to the substrate after exposure as a function of time.

3.3 Scanning electron microscopy (SEM)

As shown in Figure 9, the substrate contains microscopic defects. An ion-conducting pathway exists in the film, and the reaction sites at the interface are generated immediately upon contact with the electrolyte [22]. When the electrolyte penetrates the film, the presence of macro-defects increases the conducting pathways within the magnesium oxide film, further stimulating the transport of ions to the surface and accelerating corrosion. These results are related to those in the impedance diagrams, as it constitutes an analytical study of the various processes involved in the corrosion phenomenon. These processes manifest simultaneously, oxidizing the film and then removing it.

Figures 9 a, b and c show the surface of the material following the EIS test. Slight changes in the morphology of the surface accompany the corrosion products. This result implies that the deterioration of the material occurs evenly during the test, although the corrosion points may give way to various phenomena [23]. The morphology of the MgO coating can be observed, which includes a profile with a greater roughness and cracks present in the coating. After 90 days of immersion, the substrate exhibits a high level of cracking on the surface, which is due to differences in the crystal structures at the substrate-magnesium oxide interface.

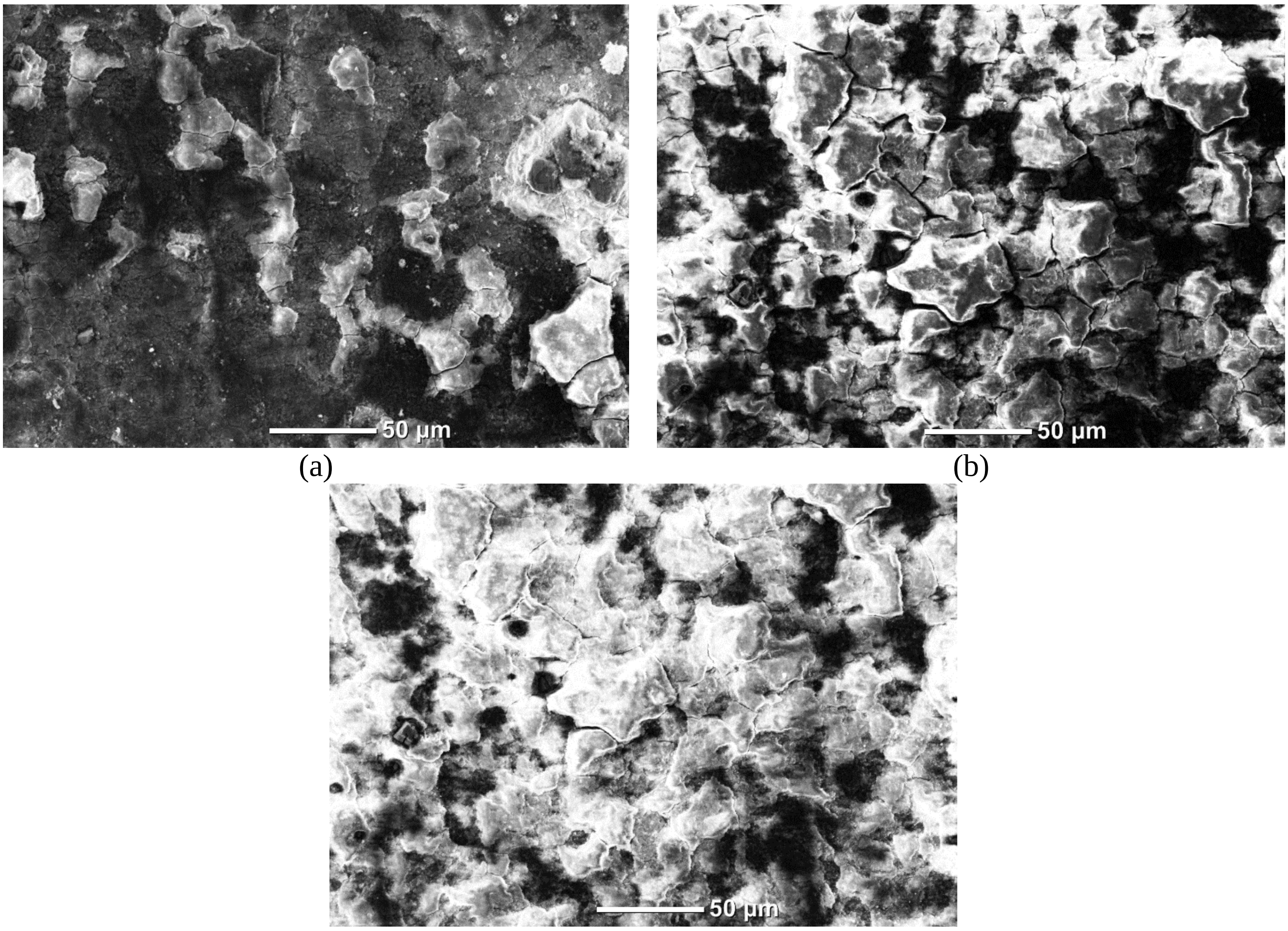

(a) (b)

(c)

Figure 9. Mg-8Er micrographs corresponding to different immersion times: a) 14 days, b) 28 days and c) 90 days.

Figure 10 shows the coatings and the corrosion protection that they offer, as no detachment is observed. The coating creates a barrier to the migration of ions before dissolving at a certain time, thereby delaying the corrosion of the metallic substrate. Figure 10a shows the morphology of the coating obtained at 14 days of exposure. The morphology is characterized by the presence of ridges and valleys with an appreciable contrast [24]. The coating is completely continuous, and the discontinuities in the central region are due to corrosion of the tricalcium phosphate that does not adhere well, which drastically changes the morphology of the coating. In Figure 10b, a homogeneous topography is observed with greater uniformity. The types of "islands" that compose the coating layer still exhibit a minor degree of roughness. This observed morphology may be associated with the dissolution of the coating as time passes because for longer times, the material tends to stabilize its surface, resulting in a slow reaction such that the ion flow in the interface promotes a minimal reaction. Figure 10c shows how the obtained coating dissolves after applying the EIS technique after 90 days. The topography is mostly uniform, which is confirmed by the ceramic characteristics of the coating being clearly distinguishable from the clear tone in the grayscale, which is suggestive of the protective nature of the coating [25].

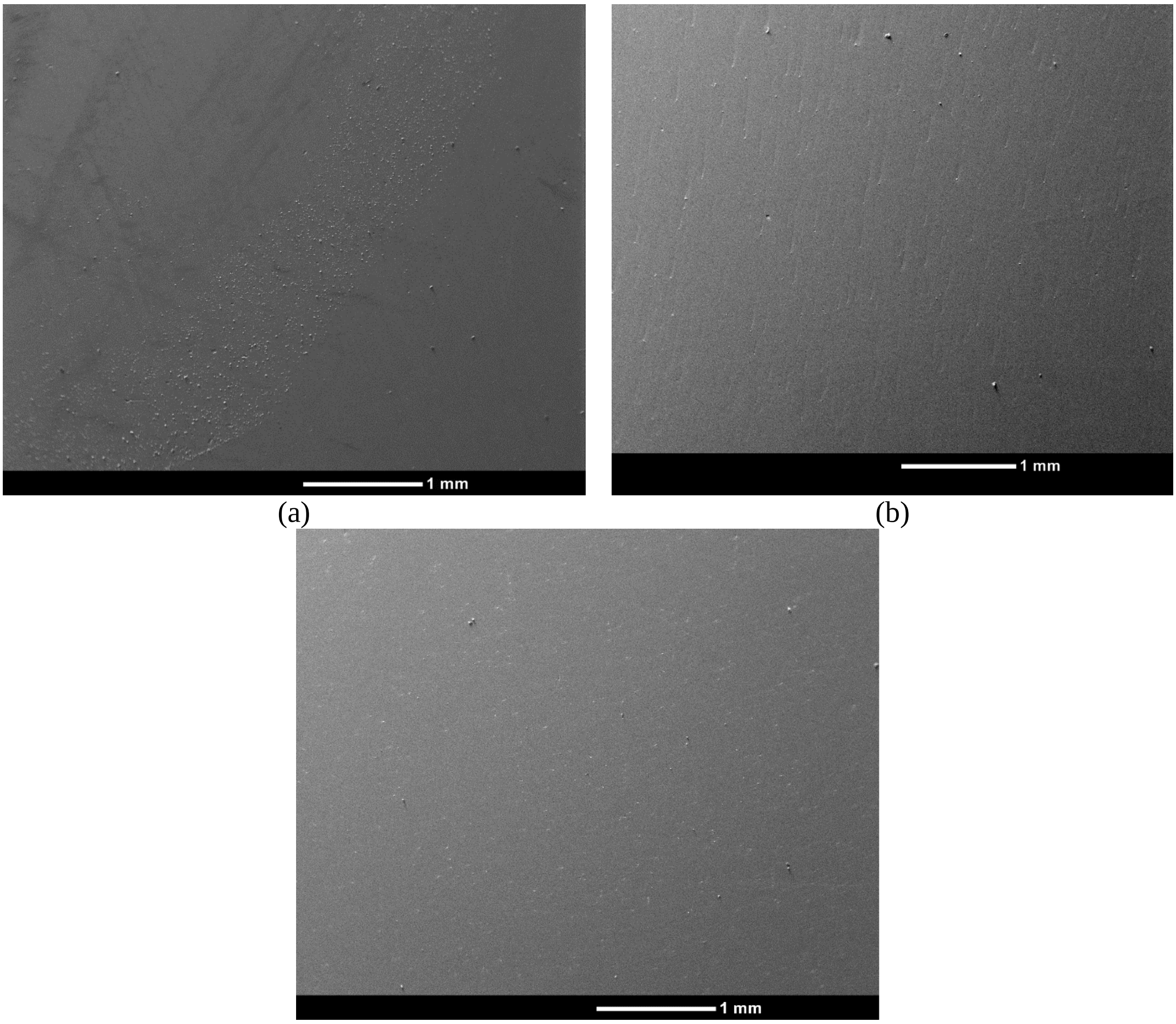

(a) (b)

(c)

Figure 10. Micrographs corresponding to the tricalcium phosphate coating after a change in topography is observed: a) 14 days, b) 28 days and c) 90 days.

4. CONCLUSIONS

The behaviour obtained after applying the EIS technique is demonstrated. The magnesium alloy generates a layer of magnesium oxide due to the interaction between the substrate and the electrolyte, which is related to their physicochemical nature and involves modifications in the anodic and cathodic regions in the electrolyte/metal interface region. For the tricalcium phosphate coating, improvements in corrosion behaviour were obtained compared to the magnesium substrate, and although it corrodes due to the saline solution in the first 28 days of evaluation, a protective layer still remains on the substrate surface. The above can be attributed to the uniform degradation increasing with the exposure time in the electrolyte. After 28 days, a barrier to ion migration is obtained, and the corrosive phenomenon decreases, promoting a longer life for the material in a physiological medium.

Using SEM and XRD characterization techniques, the corrosive nature of the substrate and the coating are observed since both techniques allow discrimination of the corrosion products and the substrate. Differences in the topography of the coatings are observed for as long as 28 days, indicating that this type of coating heterogeneity is required for the creation of an environment conducive to the degree of adhesion for the biological material that acts as a host.

ACKNOWLEDGEMENT
This research was supported by "Vicerrectoría de investigaciones de la Universidad Militar Nueva Granada" under contract ING- 2374 - 2017.

References

1. A. Morawska-Chochol, P. Domalik-Pyzik, B. Szaraniec and J. Chlopek, *Mater. Lett.*, 180 (2016) 1.
2. R. Kotoka, N. K. Yamoah, K. Mensah-Darkwa, T. Moses and D. Kumar, *Surf. Coat. Technol.*, 292 (2016) 99.
3. M. Motisuke, G. Mestres, C. O. Renó, R. G. Carrodeguas, C. A. Zavaglia and M. Ginebra, *Mater. Sci. Eng., C.*, 75 (2017) 816.
4. A. Mina, J. C. Caicedo and W. Aperador, *Int. J. Electrochem. Sci.*, 8 (2013) 11186.
5. A. Takeuchi, T. Tsuge and M. Kikuchi, *Ceram. Int.*, 42 (2016) 15376.
6. P. R. Scott, J.A. Crow, R. Z. LeGeros and M.B. Kruger, *Solid State Commun.*, 151 (2011) 1609.
7. I. Ayadi and F. B. Ayed, *J. Mech. Behav. Biomed. Mater.*, 60 (2016) 568.
8. P. N. Kumar, S. K. Mishra and S. Kannan, *J. Solid State Chem.*, 231 (2015) 13.
9. W. Liu, D. Zhai, Z. Huan, C. Wu and J. Chang, *Acta Biomater.*, 21 (2015) 217.
10. F. Pourdanesh, A. Jebali, S. Hekmatimoghaddam and A. Allaveisie, *Mater. Sci. Eng., C.*, 40 (2014) 382.
11. H. Tang, T. Xin and F. Wang, *Int. J. Electrochem. Sci.*, 8 (2013) 8115.
12. L. J. Fuh, Y. J. Huang, W. C. Chen and D. J. Lin, *Mater. Sci. Eng., C.*, 75 (2017) 798.
13. S. K. Swain, I. Gotman, R. Unger, C. J. Kirkpatrick and E. Y. Gutmanas, *J. Mech. Behav. Biomed. Mater.*, 53 (2016) 434.
14. N. Metoki, C.M.R. Rosa, H. Zanin, F.R. Marciano, N. Eliaz and A.O. Lobo, *Surf. Coat. Technol.*, 297 (2016) 51.
15. S. S. Singh, A. Roy, B. Lee and P. N. Kumta, *Mater. Sci. Eng., C.*, 64 (2016) 219.
16. K. S. Ancane, L. Stipniece, A. Putnins and L. B. Cimdina, *Ceram. Int.*, 41 (2015) 4996.
17. P.M.C. Torres, J.C.C. Abrantes, A. Kaushal, S. Pina, N. Döbelin, M. Bohner and J.M.F. Ferreira, *J. Eur. Ceram. Soc.*, 36 (2016) 817.

18. Z. Chen, X. Mao, L. Tan, T. Friis, C. Wu, R. Crawford and Y. Xiao, *Biomaterials.*, 35, (2014) 8553.
19. W. Lu, C. Ou, Z. Zhan, P. Huang, B Yan and M. Chen, *Int. J. Electrochem. Sci.*, 8 (2013) 10746.
20. I. Sallemi, J. Bouaziz and F. B. Ayed, *Mater. Chem. Phys.*, 151 (2015) 50.
21. C. Piccirillo, M.F. Silva, R.C. Pullar, I. Braga da Cruz, R. Jorge, M.M.E. Pintado and P.M.L. Castro, *Mater. Sci. Eng., C.*, 33 (2013) 103.
22. S. Kannan, F. Goetz-Neunhoeffer, J. Neubauer, S. Pina, P.M.C. Torres and J.M.F. Ferreira, *Acta Biomater.*, 6 (2010) 571.
23. X. Li, A. Ito, Y. Sogo, X. Wang and R.Z. LeGeros, *Acta Biomater.*, 5 (2009) 508.
24. M. Bobby Kannan, *Surf. Coat. Technol.*, 301 (2016) 36.
25. D. Lee, C. Sfeir and P. N. Kumta, *Mater. Sci. Eng., C.*, 29 (2009) 69.